Electric field and surface charge effects on ferroelectric domain dynamics in BaTiO_{3} single crystal

D. Y. He, L. J. Qiao, Alex A. Volinsky, Y. Bai, and L. Q. Guo

Phys. Rev. B **84**, 024101 — Published 1 July 2011

DOI: 10.1103/PhysRevB.84.024101

Electric field and surface charge effects on ferroelectric domain dynamics in $BaTiO_3$ single crystal

D.Y. He[1], L.J. Qiao[1], Alex A. Volinsky[2], Y. Bai[1], L.Q. Guo[1]

[1]*Corrosion and Protection Center, Key Laboratory for Environmental Fracture (MOE), University of Science and Technology Beijing, Beijing 100083, People's Republic of China*

[2]*Department of Mechanical Engineering, University of South Florida, Tampa FL 33620, USA*

Abstract

Potential distribution of $BaTiO_3$ single crystal ferroelectric domains was investigated by scanning Kelvin probe microscopy at room temperature with and without electric field applied parallel to (001) top surface. Immediate ***c*** domain surface potential inversion was observed after reaching 6 V/mm critical electric field intensity followed by complete recovery upon switching electric field off. Piezoresponse force microscopy was used to characterize domain structure evolution during electric field application, which caused ***c*** domain motion. Newly formed domain patterns were stable for a month after switching the electric field off. Screening surface charges and their mobility play a dominant role in this experiment.

1. Introduction

Ferroelectric perovskite oxide domain patterns are related to spontaneous polarization [1]. Screening of surface charges is a crucial phenomenon in ferroelectrics. Spontaneous polarization and the surface charge are related, thus domain charges are reflected in surface potential images [2]. Scanning probe microscopy (SPM) is a powerful tool for observing domain structures and their dynamic behavior in ferroelectric materials

at micron and nanometer scales [3-9]. As a simple and convenient non-destructive method SPM can be used to observe ferroelectric domain dynamics. Among SPM modes, scanning Kelvin probe microscopy is sensitive to electrostatic force which can be directly used to detect surface potential distribution on ferroelectric surfaces in-situ [10, 11]. Based on the piezoelectric effect, piezoresponse force microscopy (PFM) is used to characterize domain structures [12-14]. PFM main function is detecting and mapping sample local deformation in response to bias applied to the tip providing valuable insight about domain characteristics. These two modes are useful for characterizing ferroelectric domains polarization. Both Kelvin probe microscopy and PFM were used in experiments described in this paper while applying electric field to the sample.

Domain scanning probe imaging and measurements of the surface potential in ferroelectrics have been carried out by many researchers [15-25]. These studies primarily deal with the presence of adsorbates on perovskite surfaces, and observations of the surface potential inversion have been reported by several researches. Kalinin et. al. reported temperature-induced potential inversion on the $BaTiO_3$ (001) single crystal surface [15]. Liu et. al. also observed surface potential inversion after heating $LiNbO_3$ single crystal [16]. Bonnell et. al. reported surface charge effects on domain polarization surface potential characterization and domain destabilization measured by PFM [17]. This demonstrates that charges are screened on polarized ferroelectric surfaces and surface charge dynamics affects domain electric performance. The influence of surface adsorbates should be taken into account.

Here, surface potential inversion of ferroelectric domains in $BaTiO_3$ single crystal upon applying parallel electric field is reported. This phenomenon was observed in ferroelectric ***c*** domains with their spontaneous polarization pointing either up or down with respect to the top (001) surface. In this case surface charges migrated driven by applied electric field and domain polarization was obtained from surface potential imaging. The research objective was to verify whether observed surface potential

inversion is related to the actual domain switching or surface adsorbates screening. PFM was also used to characterize domain evolution during electric field application.

2. Experimental details

$BaTiO_3$ single crystal with 4×3×1 mm^3 dimensions was used in this study. The crystal was poled along [100] direction to get ***a*** domains on the (001) observed plane, and then (001) surface was polished by diamond lapping pastes and 50 nm colloidal silica suspension until the surface roughness was less than 1 nm. The sample was cleaned supersonically in deionized water for 100 seconds. After that, to obtain a multidomain structure $BaTiO_3$ crystal was heated to 135 °C for 30 minutes in air, above its 120 °C Curie temperature, and then cooled down to room temperature. This way $BaTiO_3$ polarized domain structure containing ***a***, $\boldsymbol{c}^+$ and $\boldsymbol{c}^-$ domains was achieved.

Surface potential measurements were carried out with Digital Instruments Dimension V SPM (USA) utilizing W_2C coated tip (NSG01/W_2C, NT-MDT, Russia). Experiments were performed at 135 kHz, just below the 150 kHz cantilever resonance frequency. The lift scan height in the interleave control was set to 100 nm. An oscillating voltage $V_{ac}\cos(\omega t)$ was applied directly to the cantilever tip to measure the surface potential. In these studies the driving voltage V_{ac} was 1.5 V with the scan rate of 1 Hz, thus it took 10 minutes to finish a complete surface potential image capture. In case of PFM, the same conductive tip was used. PFM mode is based on AFM contact mode, where the probe stays in permanent contact with the sample surface during imaging. To avoid damage to the tip or the sample -0.2 V set-point was used, corresponding to 364±42 nN tip-surface force, high enough to measure semiconductior I-V characteristics [18]. A 10 V peak-to-peak AC signal was applied between the probe and the sample at 15 kHz frequency, which provided the best image contrast. Mapping of the sample piezoelectric oscillation in response to externally applied electric field was detected by the lock-in amplifier. Domains with different orientation exhibited different vibration behavior,

thus domains could be distinguished from the contrast in piezoresponse images. The scan rate was 0.5 Hz, and it took 10 minutes to finish the whole image capture.

In this work, external electric field ($\boldsymbol{E_0}$) was applied paralleled to the (001) top surface. Surface potential and PFM measurements were conducted while applying different electric field. Fig. 1 shows schematics of the surface potential and PFM modes, respectively. By coating silver paste electrodes on both sides of the sample, a voltage source was connected using copper wires. Surface potential and PFM signals were measured to obtain local domain polarization evolution with applied electric field in each mode, respectively.

3. Results and Discussion

Fig. 2(a) and (b) shows topography and surface potential maps of $BaTiO_3$ (001) surface, respectively. Topography with corrugations is attributed to adjacent ***a*** and ***c*** domains. 90° ***a***-***c*** domain walls appear as vertical straight lines on the surface. Since ***c*** domain has polarization vector pointing either up ($\boldsymbol{c}^+$) or down ($\boldsymbol{c}^-$) with respect to the (001) plane, polarization charge is generated on the surface. Dark regions within the ***c*** domain with negative potential correspond to $\boldsymbol{c}^-$ domains, while the surrounding bright regions with positive potential correspond to $\boldsymbol{c}^+$ domains. 180° $\boldsymbol{c}^+$ and $\boldsymbol{c}^-$ domains are separated by irregular curved domain walls, while there is no difference between $\boldsymbol{c}^+$ and $\boldsymbol{c}^-$ domains observed in topography images. For ***a*** domain polarization vector is in the (001) plane thus it has no surface charge, so it is at zero potential and its contrast is in-between $\boldsymbol{c}^+$ and $\boldsymbol{c}^-$ domains. Bright, dark and intermediate regions correspond to $\boldsymbol{c}^-$, $\boldsymbol{c}^+$, and ***a*** domains, respectively marked in Fig. 2(b). By measuring the surface potential magnitude one can calculate the surface potential difference between $\boldsymbol{c}^+$ and $\boldsymbol{c}^-$ domains of 100 mV.

AFM topography image of $BaTiO_3$ single crystal used in experiments is shown in Fig. 1(a). It is worth noting that during testing local topography images didn't change at

all. Local surface potential images captured while applying 4 V/mm and 6 V/mm electric field intensity are shown in Fig. 1(b) and Fig. 1(c), respectively. Fig. 1(b) with 4 V/mm applied electric field intensity looks exactly as the original surface potential distribution without electric field applied. Gradually increasing electric field intensity to 4 V/mm did not cause any changes. Continued scanning was conducted for one hour for each applied electric field value. Then applied electric field intensity was continuously increased until it reached 6 V/mm. At that time, measured ***c*** domain surface potential inversed its sign, as seen in Fig. 1(c). A complete ***c*** domain sign inversion was observed. Ripples in Fig. 1(c) are simply noise caused by applied electric field not related to the intrinsic domain structure because these ripples change orientation with the scanning direction. Variation of the surface potential is seen by comparing Fig. 1(b) and 1(c), where positive charge areas (bright zones) become negative (dark zones), although potential magnitude was much lower than the original value. Above this 6 V/mm electric field intensity critical value, up to 8 V/mm, no further change in the surface potential was observed.

It appears that complete sign change of $\boldsymbol{c}^{+}$ and $\boldsymbol{c}^{-}$ domains occurred as if they switched places with each other. It is important to understand this domain switching behavior. New domains can nucleate and polarized domains can change their orientation due to external loading in terms of external electric field, or stress. Based on a previous domain switching study [26], it is typically accompanied by domain nucleation and growth process after reaching 200 V/mm coercive field intensity. However, during this 6 V/mm applied electric field surface potential measurement, domain switching happened in a very short time without domain walls movement, seen from potential mapping in Fig. 2(c). Here surface potential inversion did not follow typical domain switching mechanisms. Thus it is obvious that the surface potential inversion did not happen because of the actual domain switching, but rather reflects surface charges related to surface polarization.

Based on X-ray photoelectron spectroscopy and PFM measurements, $BaTiO_3$

surface layer consists of chemisorbed and physisorbed species [26]. One way to remove adsorbates is heating the sample to relatively high temperatures, however, complete adsorbates removal from $BaTiO_3$ surface is impossible [26]. Defects such as O vacancies are preferred chemisorbtion locations [23]. Strong chemical bonds with both BaO and TiO_2 terminations also induce chemisorption. Geneste and Dkhil found through density-functional calculations that in-plane-polarized $BaTiO_3$ (001) surface has strong interactions with water chemisorbed on both BaO and TiO_2 terminations [28]. Thus on $BaTiO_3$ surface strong interactions and immobile chemisorption happen by electron transfer of a chemical bond. On the other hand, highly mobile surface screening charges appeared due to physisorption on polarized domain surface to reduce depolarization field [29]. They are adsorbed on the surface by means of attractive forces from oriented dipoles, similar to our previous study of water adsorption on $BaTiO_3$ single crystal [30]. These attractive forces have a strong effect on the spread of ferroelectric surface charge. Adsorbed charges on the oxide surface are removable. Low activation energy of 4 kJ/mole [15] suggests that regardless of the interaction between adjacent screening charges the energy of a single mobile charge is only 0.04 eV. Thus immediate desorption can easily happen due to applied electric field and charges diffusion process was observed. At any point of the image the effective electric field, $\boldsymbol{E_{eff}}$, can be estimated as:

$$\boldsymbol{E_{eff}}=\boldsymbol{E_0}+\boldsymbol{E_a}+\boldsymbol{E_d} \quad (1).$$

Here, $\boldsymbol{E_0}$ is an externally applied electric field, $\boldsymbol{E_a}$ is an intrinsic field related to the ferroelectric symmetry breakdown or anisotropy field, and $\boldsymbol{E_d}$ is depolarizing field induced by bound charges. Thus obtained effective electric field is dramatically decreased compared with the externally applied electric field. In our test 6 V/mm applied electric field intensity was reduced to 2 V/mm, based on the actual surface potential measurements. Although 6 V/mm reversal electric field intensity is low compared with 200 V/mm coercive field intensity [31, 32], the effective electric field is still sufficient to mobilize screening charges on the surface. Although physisorbed species are removed,

chemisorbed charges stay on the surface to compensate depolarizing field. Immobile charges or adsorbates remain on the surface to compensate the polarized state. When electric field is switched off, surface compensation returns to the charge screening state. Again, surface potential recovers to the original value, since the electric field-dependent surface potential mainly relies on the adsorption and desorption of the surface screening charges.

As an alternative explanation, it has been reported that stable domain polarization distribution wouldn't change until the surface compensation charge density exceeds a critical 0.7-0.8 C/m^2 value based on the phase field model [33]. During the experiment, after the mobile charges detached from the surface while electric field was applied, the surface charge screening state was changed. In the absence of mobile charges, the surface charge density decreased to a partially screened state. As a result measured surface potential sign was reversed. However, after mobile charges removal, charge density still didn't pass the critical value which could still sustain the original domain polarization by compensation of the ferroelectric surface, thus no domain wall movement was observed and no new domains appeared.

In order to understand mobile charges behavior on ferroelectric surface, PFM was utilized to characterize surface charge dynamics effects on ferroelectric domain inversion during electric field application. One-hour continued scanning was conducted for each value of applied electric field. After one hour of scanning without electric field applied, no changes appeared in PFM images. After one hour of testing with 2 V/mm applied electric field intensity there was still no change in domain structure. When applied electric field intensity was increases to 4 V/mm, during the first 20 minutes no obvious changes occurred. Consequently ***c*** domain structure gradually changed with time. The 180° ***c*** domain wall was removed. After 90 minutes of scanning the ***c*** domain structure was changed significantly, whereas ***a*** domain did not change throughout the whole scanning period. Another ***a-c*** domain area was selected for PFM scanning, and with 6

V/mm applied electric field intensity, PFM image changed more dramatically in Fig. 3. Only after 3 complete image captures in 30 minutes, all $\boldsymbol{c}^+$ domains changed to $\boldsymbol{c}^-$ domains. While significant ***c*** domain mobility was observed, ***a*** domain did not change. Bonnell et. al found that under UV illumination domain walls move rapidly during PFM scanning [17]. We observed the same behavior when parallel electric field was applied to the sample during PFM scanning. Furthermore, inspection of a larger image of the measured zone in Fig. 3(d) reveals that the domain motion is mainly induced by the tip scanning, since only the previously scanned area underneath the tip was involved in domain evolution. An obvious square in the middle of Fig. 3(d) is the scanning area where PFM measurements were performed earlier. Larger area outside of the previously scanned square remains unmodified, exhibiting the same features as in the beginning of the experiment.

In Fig. 4 $\boldsymbol{c}^+$ domain area dependence on scanning time at 4 V/mm and 6 V/mm is plotted, showing $\boldsymbol{c}^+$ domain switching to $\boldsymbol{c}^-$ domain. Domain evolution was more rapid with higher applied electric field. After switching the electric field off, newly achieved ***a-c*** domain structure was stable and didn't change even after one month of storage.

When electric field was applied, it stimulated the surface screening charge on polarized ***c*** domain leading to surface charge migration. During PFM imaging, AFM tip with a conductive coating stays in contact with the surface. Removed mobile charges migrated along the tip and gathered at the end of the tip, thus a high local electric field was formed between the tip and the sample. Higher 6 V/mm applied electric field intensity moved the screening charges easier, so in a very short time gathered charges formed large enough local tip electric field leading to faster and more dramatic domain motion compared with lower 4 V/mm applied electric field intensity. In case of 4 V/mm, surface screening charges already possess certain energy that does not exceed the physisorption energy agreeing with no surface potential switching. However, conductive tip in contact with ferroelectric surface stimulates the charges, thus after 20 minutes of

inactivity domains start to move. Furthermore, at 4 V/mm domain motion is much slower than at 6 V/mm applied electric field intensity, seen in Fig. 4. For ***a*** domain, there is no screening charge on the surface, so when the tip scanned ***a*** domain region, there was no mobile screening charge gathered, although electric field was applied to the sample. Thus no local electric field was generated between the tip and the sample resulting in no ***a*** domain change. It turns out that PFM scanning-induced domain evolution was not only related to the electric field applied to the sample but also to the polarization state of the domain. Surface charges screening and their mobility play a dominant role in described experiments.

4. Conclusions

In summary, surface potential evolution on (001) $BaTiO_3$ single crystal surface with electric fields applied along the [010] direction was studied. A strong influence of the electric field on the surface potential of $BaTiO_3$ domain was found. Surface potential sign of ***c*** domains inversed as soon as applied electric field intensity reached 6 V/mm and switched back after the electric field was turned off. This electric field-dependent surface potential mainly relies on the adsorption and desorption of the surface screening charges driven by the low 4 kJ/mole activation energy. Surface potential exhibited inversion because of the surface charge dispersion on the surface. Domain motion induced by PFM scanning while applying electric field was caused by removing screening charge accumulated at the end of the tip. Local electric field was generated between the tip and the sample leading to domain evolution in PFM mode where conductive tip stays in contact with the sample surface.

Acknowledgments

Authors acknowledge support from the National Nature Science Foundation of China under grants 51072021 and 50632010 and from Beijing Municipal Commission of

Education under YB20091000801 grant. Alex Volinsky acknowledges support from the National Science Foundation under 1000138 and 0966248 grants.

References

[1] D.Vanderbilt, Phys. Rev. B. 41, 7892 (1990).

[2] S.V. Kalinin and D.A. Bonnell, Phys. Rev. B. 63, 125411 (2001).

[3] Y.G. Wang, J. Dec and W. Kleemann, J. Appl. Phys. 84, 6795 (1998).

[4] J. Munoz-Saldana, G.A. Schneider, and L.M. Eng, Surf. Sci. 480, L402 (2001).

[5] B. Reichenberg, S. Tiedke, K. Szot, F. Peter, R. Waser, S. Tappe, and T. Schneller, J. Eur. Ceram. Soc. 25, 2353 (2005).

[6] B.J. Rodriguez, R.J. Nemanich, A. Kingon, and A. Gruverman, Appl. Phys. Lett. 86, 012906 (2005).

[7] Y.B. Park, M.J. Dicken, Z.H. Xu, and X.D. Li, J. Appl. Phys. 102, 083507 (2007).

[8] O.S. Ovchinnikov, S. Jesse, S.V. Kalinin, Nanotechnology. 20, 255701 (2009).

[9] S.V. Kalinin, A.N. Morozovska, L.Q. Chen, and B.J. Rodriguez, Rep. Prog. Phys. 73, 056502 (2010).

[10] Q. Zhang, C.H. Kim, Y.H. Jang, H.J. Hwang, and J.H. Cho, Appl. Phys. Lett. **96**, 152901 (2010).

[11] Y. Kim, M. Park, S. Buhlmann, S. Hong, Y.K. Kim, H. Ko, J. Kim, and K. No, J. Appl. Phys. **107**, 054103 (2010).

[12] F. Peter, A. Rüdiger, and R. Waser, Rev. Sci. Instrum. **77**, 036103 (2006).

[13] A.N. Morazovska, E.A. Eliseev, and S.V. Kalinin, J. Appl. Phys. **102**, 074105 (2007).

[14] T. Jungk, Á. Hoffmann, and E. Soergel, Appl. Phys. Lett. **89**, 163507 (2006).

[15] S.V. Kalinin, C.Y. Johnson, and D.A. Bonnell, J. Appl. Phys. 91, 3816 (2002).

[16] X.Y. Liu, K. Kenji, and T. Kazuya, Appl. Phys. Lett. 89, 132905 (2006).

[17] R. Shao, M.P. Nikiforov, and D.A. Bonnell, Appl. Phys. Lett. **89**, 112904 (2006).

[18] M. Li, Y.J. Su, W.Y. Chu, L.J. Qiao, A.A. Volinsky, G. Kravchenko, Appl. Phys. Lett. **98**(8), 082105 (2011).

[19] Q. Dai, J. Hu, and M. Salmeron, J. Phys. Chem. B **101**, 1994 (1997).

[20] M. Luna, J. Colchero, and A.M. Baro, J. Phys. Chem. B **103**, 9576 (1999).

[21] M. Luna, J. Colchero, A. Gil, J. Go´mez-Herrero, and A.M. Baro, Appl. Surf. Sci. **175**, 393 (2000).

[22] A. Verdaguer, M. Cardellach, and J. Fraxedas, J. Chem. Phys. **129**, 174705 (2008).

[23] D.B. Li, M.H. Zhao, J. Garra, A.M. Kolpak, A.M. Rappe, D.A. Bonnell, and J. M. Vohs, Nature Mater. 7, 473 (2008).

[24] S.V. Kalinin and D.A. Bonnell, Appl. Phys. Lett. **78**, 1116 (2001).

[25] S. Shin, J. Baek, J.W. Hong, and Z.G. Khim, J. Appl. Phys. **96**, 4372 (2004).

[26] B. Jiang, Y. Bai, W.Y. Chu, L.J. Qiao. Appl. Phys. Lett., **93**, 152905 (2008)

[27] F. K. Szot, R. Waser, B. Reichenberg, S. Tiedke, and J. Szade, Appl. Phys. Lett. 85, 2896 (2004).

[28] G. Geneste and B. Dkhil, Phys. Rev. B **79**, 235420 (2009).

[29] S.V. Kalinin and D.A. Bonnell, J. Appl. Phys. **87**, 3950 (2000).

[30] D.Y. He, L.J. Qiao, A.A. Volinsky, Y. Bai, M. Wu, W.Y. Chu, Appl. Phys. Lett. **98**(6), 062905 (2011)

[31] W.J. Merz, Phys. Rev. 95, 650 (1954).

[32] A. Ryuji, J. Phys. Soc. Jpn. 15, 795 (1960).

[33] J. Wang and M. Kamlah, Appl. Phys. Lett. 93, 262904 (2008).

Figures

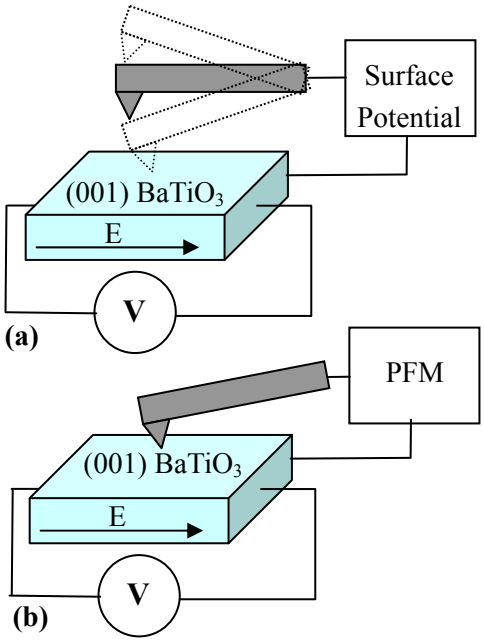

Fig. 1. (a) Schematic of the surface potential measurements with electric field applied along (001) $BaTiO_3$ surface. (b) Schematic of PFM measurements.

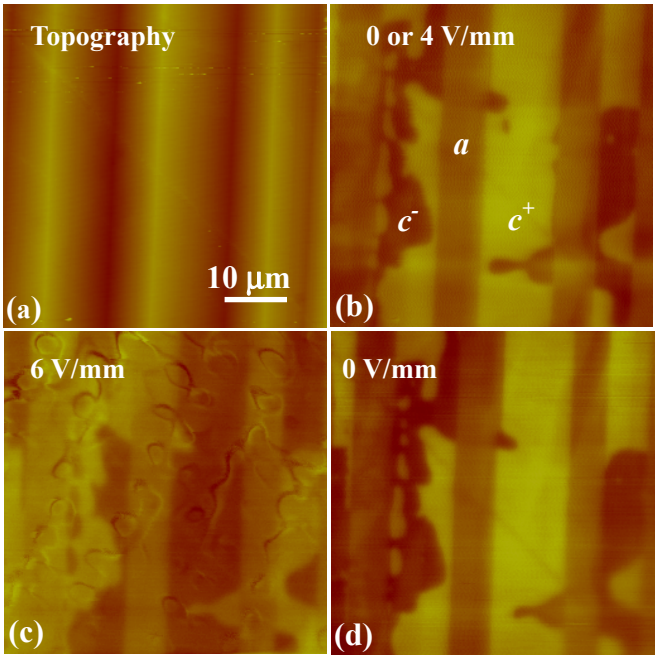

Fig. 2. (a) AFM local topography image of (001) $BaTiO_3$ surface with 200 nm Z scale. (b) Surface potential image without voltage applied or with 4 V/mm applied electric field intensity. (c) Surface potential image after applying 6 V/mm electric field intensity showing surface potential inversion. (d) Complete recovery upon switching off the electric field.

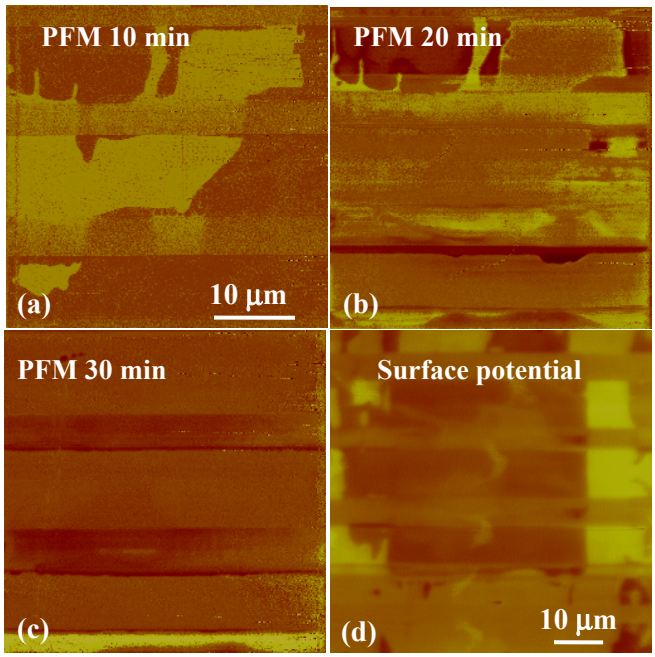

Fig. 3. PFM images of domain structure on (001) $BaTiO_3$ single crystal showing domain evolution with 6 V/mm electric field intensity applied to the sample for: (a) 10 min, (b) 20 min and (c) 30 min. (d) Larger surface potential image showing zoomed out area.

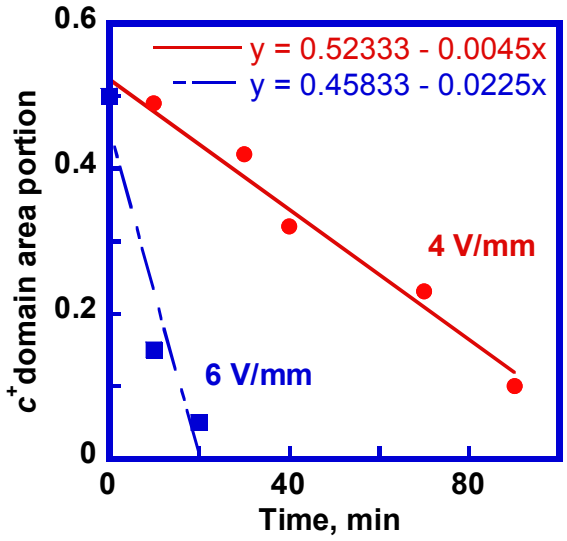

Fig. 4. $\boldsymbol{c}^+$ domain area portion of the total $\boldsymbol{c}$ domain area for 4 V/mm and 6 V/mm applied electric field intensities. Originally $\boldsymbol{c}^+$ domains occupied half of the $\boldsymbol{c}$ domain area, and later switched to $\boldsymbol{c}^-$ domains.